Colloids and Surfaces B: Biointerfaces 192 (2020) 111053

Contents lists available at ScienceDirect

Colloids and Surfaces B: Biointerfaces

journal homepage: www.elsevier.com/locate/colsurfb

Size Measurement of Extracellular Vesicles and Synthetic Liposomes: The Impact of the Hydration Shell and the Protein Corona

Zoltán Varga[a,*], Bence Fehér[a,b], Diána Kitka[a], András Wacha[a], Attila Bóta[a], Szilvia Berényi[c], Vitaliy Pipich[d], Jean-Luc Fraikin[e]

[a] Biological Nanochemistry Research Group, Institute of Materials and Environmental Chemistry, Research Centre for Natural Sciences, Magyar tudósok körútja 2, H-1117 Budapest, Hungary
[b] Institute of Chemistry, Eötvös Loránd University, Pázmány Péter sétány 1/A, H-1117 Budapest, Hungary
[c] BME Chemical Nanosensors Research Group, Department of Inorganic and Analytical Chemistry, Budapest University of Technology and Economics, Szent Gellért tér 4. H-1111 Budapest, Hungary
[d] Jülich Centre for Neutron Science JCNS at Heinz Maier-Leibnitz Zentrum, Forschungszentrum Jülich GmbH, Lichtenbergstraße 1, 85747 Garching, Germany
[e] Spectradyne LLC, 23875 Madison St, Suite A, 90505 Torrance, CA, USA

ARTICLE INFO

Keywords:
exosome
microparticle
liposomal drug delivery
small-angle neutron scattering
microfluidic resistive pulse sensing

ABSTRACT

Size characterization of extracellular vesicles (EVs) and drug delivery liposomes is of great importance in their applications in diagnosis and therapy of diseases. There are many different size characterization techniques used in the field, which often report different size values. Besides technological biases, these differences originate from the fact that various methods measure different physical quantities to determine particle size. In this study, the size of synthetic liposomes with nominal diameters of 50nm and 100nm, and red blood cell-derived EVs (REVs) were measured with established optical methods, such as dynamic light scattering (DLS) and nanoparticle tracking analysis (NTA), and with emerging non-optical methods such as microfluidic resistive pulse sensing (MRPS) and very small-angle neutron scattering (VSANS). The comparison of the hydrodynamic sizes obtained by DLS and NTA with the sizes corresponding to the excluded volume of the particles by MRPS enabled the estimation of the thickness of the hydration shell of the particles. The comparison of diameter values corresponding to the boundary of the phospholipid bilayer obtained from VSANS measurements with MRPS size values revealed the thickness of the polyethylene glycol-layer in case of synthetic liposomes, and the thickness of the protein corona in case of REVs.

1. Introduction

The field of nanomedicine has grown rapidly since liposomal drugs were first clinically approved in the 1990s, and its growth has accelerated over the last decade as extracellular vesicles (EVs) have shown significant diagnostic and therapeutic promise because of the key roles they play in intercellular communication (1–5). Due to their low immunogenicity and natural homing ability, EVs may represent the next generation of lipid-based drug delivery systems (6).

Both drug delivery liposomes and extracellular vesicles (EVs) are spherical phospholipid bilayer structures with diameter spanning from about 30 nanometers to several hundred nanometers. Accurate size measurement of liposomes and EVs is prerequisite for realizing their full potential in clinical applications (7–10). In general, size characterization methods can be grouped according to their measurement principle into ensemble and single-particle detection methods. Dynamic light scattering (DLS) is the most widely used ensemble method for the sizing of nanoparticles (7,11). Small-angle X-ray and neutron scattering (SAXS and SANS, respectively) belong also to the group of ensemble methods used for the sizing of lipid vesicles (12–17). On the other hand, transmission and cryo- electron microscopy (TEM and cryo-EM) are the most significant examples for single-particle detection methods that are used to characterize liposomes (8,11) and also EVs (18–20). Atomic force microscopy (AFM) and resistive pulse sensing (RPS, or scanning ion occlusion sensing, SIOS) are also frequently used single-particle methods both in the liposome- and the EV-fields (21–24). Sizing methods can be also classified based on their physical principles. In this regard, optical and non-optical methods are usually distinguished. DLS mentioned above belongs to the optical methods, but nanoparticle tracking analysis (NTA) (25,26) and flow cytometry (FCM) (27–31)

* Corresponding author:
E-mail address: varga.zoltan@ttk.hu (Z. Varga).

https://doi.org/10.1016/j.colsurfb.2020.111053
Received 29 November 2019; Received in revised form 16 March 2020; Accepted 12 April 2020
Available online 19 April 2020

should be also listed as optical methods for single particle detection of liposomes and EVs.

The various methods for sizing liposomes and EVs have been compared in recent studies and often report different average size values (23,29,32,14). These differences are due to methodological biases including the response of different techniques to sample heterogeneity, the small size limits of detection of the methods, and fundamental differences in the physical properties being measured between the techniques.

In general, ensemble methods are only accurate for measuring monodisperse samples, since for a heterogeneous sample the calculation of the size distribution from the primary measured quantity becomes an ill-posed inverse mathematical problem. For example, a plurality of heterogeneous particle size distributions could give rise to the same correlation function measured by DLS or scattering curve measured by SAXS/SANS. Methods that independently measure single particles in a sample do not suffer from this limitation.

The sensitivity limit of any metrology is a critical parameter that must be understood for any measurement. For example, in case of NTA, the most common optical single-particle sizing method, the small size limit of detection (LOD) is determined by the light scattering cross-section, which scales very strongly with particle diameter and depends in a complex way on the material composition of the particles in the sample being measured. As a result, the LOD of NTA depends on the sample itself in a way that cannot be fully understood without independent measurements made using truly orthogonal methods. The impact of this inherent uncertainty is amplified by the data presentation format, which commonly spans an unphysical range starting at zero nm diameter. These factors affect 'average' particle sizes reported in the literature.

Finally, various methods measure different physical quantities to determine particle size, leading to further variation in the reported size values. A striking example for the latter is the comparison of DLS and TEM: DLS measures the autocorrelation function of the laser intensity scattered from the sample at a fixed angle. The primary information from the autocorrelation function is the diffusion coefficient of the examined particles, which is used to calculate the so-called hydrodynamic diameter of the particles according to the Stokes-Einstein equation. Since the diffusion of the particles is affected by their interfacial properties (e.g. hydration and organic capping layer on the surface), the reported size exceeds the hard boundary of the particles under investigation. On the other hand, TEM provides an image of the electron density inhomogeneities in the sample. The electron density contrast between the core of the particles and its hydration or organic capping shell is usually significant, which implies that size values reported by TEM are closer to the core size of the particles.

In this paper we demonstrate that combining measurements from complementary and orthogonal particle sizing techniques provides new information about the structural features of vesicular nanoparticles that amounts to more than the sum of the individual measurements. Two types of vesicular samples were measured: Polyethylene glycol (PEG)-grafted, sterically stabilized liposomes (SSL) used for drug delivery and red blood cell-derived EVs (REVs). Measurement techniques included two well established methods (DLS and NTA) and two new emerging methods (Very Small-Angle Neutron Scattering (VSANS) and Microfluidic Resistive Pulse Sensing (MRPS)). This choice of measurement techniques covers all four groups of size characterization methods: Ensemble and single-particle characterization methods and optical and non-optical operating principles. We hypothesized that important quantities such as the thickness of the PEG-layer in case of drug delivery liposomes, or the protein corona in case of REVs can be investigated by the comparison of various sizing techniques. The latter is gaining attention in the field of EVs as the protein corona affects not only the biodistribution of EVs but also their detection and quantification. The PEG-layer in case of SSLs is responsible for avoiding the fast clearance of these drug delivery vehicles from the blood circulation, therefore its characterization for new liposomal drugs is vitally important.

2. Materials and Methods

2.1. Liposome preparation

Hydrogenated soy phosphocholine (HSPC, Coatsome NC-21E), 1,2-distearoyl-sn-glycero-3-phosphoethanolamine-N-[methoxy(polyethylene glycol)-2000] (DSPE-PEG2k, 880120 P) were purchased from NOF Corporation (Japan) and from Avanti Polar Lipids (USA), respectively. Cholesterol (C8667), phosphate buffered saline (PBS, P3813), and heavy water (D_2O, 151882) were purchased from Sigma-Aldrich (Hungary). All chemicals were used without further purification. Sterically stabilized liposome (SSL) samples were prepared by the hydration, freeze-thaw and extrusion method. Briefly, the components were dissolved in chloroform in weight ratio of HSPC:DSPE-PEG2k:Cholesterol = 3:1:1. The solvent was then evaporated at 40 °C and the resulting lipid film was kept in vacuum overnight to remove residual traces of the solvent. PBS buffer solution made of ultrapure water (18.2 MΩ cm) or D_2O (in case of the samples for neutron scattering experiments) was added to the samples to gain a total lipid concentration of 16 mg/ml. Ten freeze-thaw cycles by using liquid nitrogen and lukewarm water bath were applied for homogenization. Finally, the samples were extruded (at 60 °C) ten times through polycarbonate filters with 50 nm or 100 nm pore sizes (110603 and 110605, respectively, Nuclepore, Whatman Inc.), for SSL 50 and SSL 100 samples, respectively, using a LIPEX extruder (Northern Lipids Inc., Canada).

2.2. Isolation of red blood cell (RBC)-derived extracellular vesicles (REVs)

EDTA-anticoagulated blood was collected from healthy volunteers (3 x 6 mL) with informed consent by venepuncture without a tourniquet through a 21-gauge needle by use of a vacutainer system (456036, Geiner Bio-One, Hungary). The use of human blood samples was approved by the Scientific and Research Ethics Committee of the Hungarian Medical Research Council (ETT TUKEB 6449-2/2015). Whole blood was centrifuged at 2500 x g for 10 min (Nüve NF 800R centrifuge, swing-out rotor) then the plasma and the white blood cell fractions were removed and RBCs were suspended in equal volume of saline solution (0.9%) and washed three times at 2500 x g 10 min at 4 °C. After washing, RBCs were diluted with equal volume of phosphate buffered saline pH 7.4 (PBS, P3813, Sigma-Aldrich, Hungary) and were kept at 4 °C for 7 days. At the end of the incubation period, the RBCs were removed by centrifugation at 1500 x g for 10 min followed by another centrifugation step at 2850 x g for 30 min. The RBC-free supernatant was aliquoted into 2 mL Eppendorf tubes and pelleted at 16 000 x g for 30 min (Eppendorf 5415R, F45-24-11 rotor, Austria). Each pellet was resuspended in 100 µl PBS. The REV sample was further purified with SEC using a 3.5 mL gravity column filled with Sepharose CL-2B gel (17014001, GE Healthcare, Sweden). 100 µl REV sample was pipetted onto the column which was followed by 900 µl PBS (prepared with ultrapure water or D_2O for the VSANS measurements), while the flow through was discarded. Next, the purified REVs were eluted with 1 mL PBS and collected. Purified samples were stored at 4 °C and were used within 48 hours after isolation.

2.3. Freeze-fracture combined transmission electron microscopy (FF-TEM)

Sample were mixed with glycerol (G5516, Sigma-Aldrich, Hungary) used as cryoprotectant at 3:1 sample-to-glycerol volume ratio. Approx. 2 µL sample was pipetted onto a gold sample holder and frozen by placing it immediately into partially solidified Freon for 20 seconds. Fracturing was performed at −100 °C in a Balzers freeze-fracture device (Balzers BAF 400D, Balzers AG, Liechtenstein). The replicas of the

fractured surfaces were made by platinum-carbon evaporation and then cleaned with a water solution of surfactant and washed with distilled water. The platinum-carbon replicas were placed on 200 mesh copper grids and examined in a MORGAGNI 268D (FEI, The Netherlands) transmission electron microscope.

2.4. Dynamic light scattering (DLS)

DLS measurements were performed using a W130i apparatus (Avid Nano Ltd., UK) and using a low volume disposable cuvette (UVette, Eppendorf Austria GmbH, Austria).

2.5. Nanoparticle tracking analysis (NTA)

NTA measurements were performed using a NanoSight LM10-HS system (Malvern Instruments Ltd., UK) equipped with a 488 nm laser module. All measurements were performed at room temperature, and the camera level vas set to 16. Results were evaluated as an average five 10 s duration track record using NanoSight NTA software version 2.3. Samples were diluted in PBS filtered through a VivaSpin 500, 100 kDa MWCO membrane filter (VS0141, Sartorius, Germany) according to the manufacturer's instructions.

2.6. Microfluidic resistive pulse sensing (MRPS)

MRPS measurements were performed with a nCS1 instrument (Spectradyne LLC, USA). SSL and REV samples were diluted 10000-fold and 10-fold, respectively, with bovine serum albumin (BSA, A2153, Sigma-Aldrich, Hungary) solution at 1 mg/mL in PBS buffer, filtered through a VivaSpin 500, 100 kDa MWCO membrane filter (Sartorius, Germany) according to the manufacturer's instructions. The SSL 50 sample was measured with a TS-300 cartridge (50 nm to 300 nm measurement range), while SSL 100 and REV samples were measured with TS-400 cartridges (65 nm to 400 nm measurement range).

2.7. Very-small angle neutron scattering (VSANS)

VSANS experiments were carried out at the KWS-3 instrument operated by Jülich Center for Neutron Sciences (JCNS) at the FRM-II research reactor (Heinz Maier-Leibnitz Zentrum, MLZ, Garching, Germany) (38,39). SSL and REV samples prepared in PBS-D_2O were filled into standard Hellma cells (404-QX, Hellma GmbH & Co. KG, Germany), measured at room temperature at sample positions of 9.5 m and 1.3 m sample-to-detector distances to cover the q-range from $4{\cdot}10^{-3}$ nm^{-1} to $2{\cdot}10^{-1}$ nm^{-1}. Radial averaging of the 2D scattering patterns, background subtraction and calibrations for intensity and scattering variable, q, were performed by QtiKWS10 software provided at the beam line.

Model fitting procedures using core-shell and solid-sphere models were carried out using a self-developed software written in Python. Details are provided in the Supplementary Information.

3. Results and Discussion

Freeze-fracture combined TEM (FF-TEM) provides an excellent tool to visualize individual vesicles suspended in an aqueous medium. Fig. 1 shows typical FF-TEM images of the investigated SSL and REV samples. All samples exhibit uniform particles with close to the regular spherical shape. The surface morphology of SSLs prepared by using membrane filters with nominal pore size of 50 nm (SSL 50) and 100 nm (SSL 100) definitively differs from that of the REV sample. Smooth outer and inner surfaces can be observed in the pictures of SSL 50 and SSL 100 samples shown in Fig. 1(a–c) and (d–e), respectively. In contrast, the surface of the REV sample is randomly and densely covered with small particles (Fig. 1f–h), which fall in the 5 to 15 nm size range. These particles can be attributed to the membrane proteins on the surface of REVs. The inner surface of REVs contains significantly less protein associates than the outer one (Fig. 1g,h). The average estimated size of the SSL 50, SSL 100 and REV samples is 80 nm, 120 nm and 200 nm, respectively. While the size of the liposomes and REVs can be distinguished based on the FF-TEM images, quantitative size distributions cannot be obtained because of the limited number of liposomes and REVs on the images, and because fracturing takes place at a diameter equal to or less than the maximal diameter.

DLS, NTA and MRPS analysis of the investigated samples are shown in Fig. 2. DLS, the most frequently used routine optical ensemble technique reports a similar trend for mean particle size in the three samples as was observed by FF-TEM. However, since DLS measures the average hydrodynamic diameter of the particles the mean diameter measurements are shifted towards larger values (Fig. 2b). DLS mean hydrodynamic diameters of the SSL 50, SSL 100 and REV samples were (101.9 ± 2.0) nm, (123.2 ± 3.8) nm, and (225.6 ± 6.7) nm respectively (± standard deviation, N = 3). The correlation functions shown in Fig. 2a are consistent with relatively monodisperse samples and suggest the absence of aggregates.

NTA is an optical, single-particle method that tracks the Brownian motion of individual particles suspended in a liquid using their scattered light. The hydrodynamic size of each diffusing particle is inferred from its measured mean squared displacement and an assumption of the viscosity of the suspending medium. Size distributions of the SSL and REV samples obtained by NTA are shown in Fig. 2c, and mean hydrodynamic diameter values agree within a few nanometers of those measured by DLS: (96.0 ± 1.7) nm, (115.0 ± 1.8) nm, and (216.0 ± 3.2) nm for the SSL 50, SSL 100 and REV samples, respectively for NTA (± standard deviation, N = 5). These results indicate that for such monodisperse samples as the SSLs and REVs, the ensemble technique measures an average hydrodynamic diameter that agrees with the same physical quantity measured by the single-particle detection method.

Size distributions of the investigated samples measured by MRPS are shown in Fig. 2d. MRPS is the nanoscale implementation of the Coulter principle in a microfluidic cartridge (33–35), as such, it is a non-optical, single-particle detection method. The particle size distributions measured by MRPS are approximately Gaussian and show significantly smaller size values compared to those obtained by DLS and NTA: Mean particle diameters calculated from the MRPS particle size distributions for the SSL 50, SSL 100 and REV samples were (70.3 ± 3.2) nm, (95.5 ± 0.9) nm, and (186.1 ± 9.2) nm respectively. Unlike DLS and NTA however, MRPS does not measure hydrodynamic radius. Instead, MRPS measures the volume of conductive ions excluded by each particle as it passes through a constriction in the fluid flow. In the case of a closed core particle coated with a hydrated PEG layer, the PEG layer significantly affects the mobility of the particle and thus increases its hydrodynamic diameter. For the same particle, MRPS will report a diameter that is closer to and slightly larger than the core diameter size reported by TEM. This physical understanding is supported by the data: Both DLS and NTA report similar values for mean hydrodynamic diameter despite significantly different data analysis procedures, and the TEM and MRPS results are in agreement.

This interpretation of the combined physical measurements then allows an estimate of the hydration shell thickness. Using the MRPS values as the 'core' particle size and the hydrodynamic diameters obtained by DLS and NTA as the 'outer' hydrated diameter, the hydration shell thickness is calculated to be 10 nm to 16 nm for the SSL samples, and from 15 nm to 20 nm for the REV sample. For SSLs, these results agree with prior measurements of liposomal doxorubicin by Peretz et al. in which diameters from DLS measurements and from cryo-EM investigations supplemented with PEG-layer thickness values from SAXS were compared (8). In case of REVs, the large hydrodynamic diameter can be attributed to the protein agglomerates on their surface.

The fourth technique used in this study for the size characterization of vesicle systems was VSANS, which is an ensemble method. In VSANS,

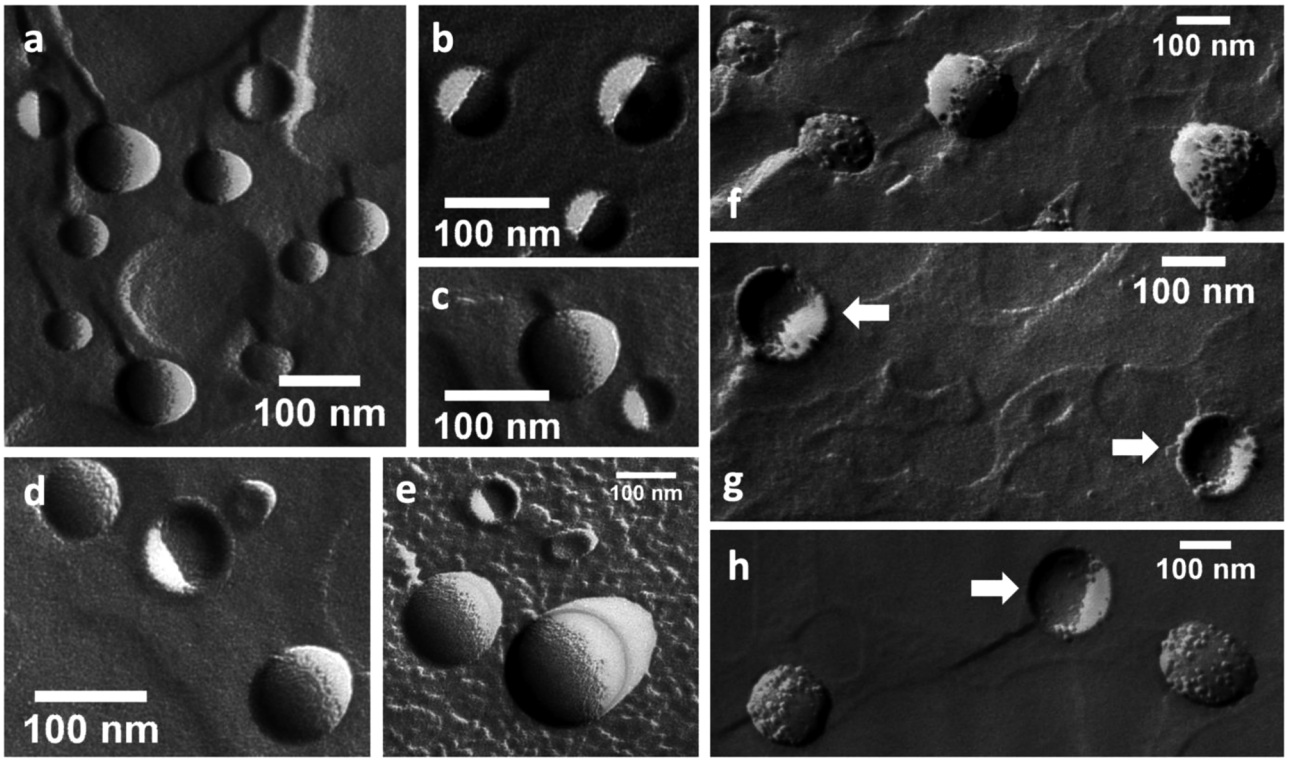

Fig. 1. Freeze-fracture TEM images of sterically stablized liposomes (SSLs) prepared by using membrane filters with nominal pore size of 50 nm (SSL 50, a-c) and 100 nm (SSL 100, d-e) and red blood cell derived extracellular vesicles (REVs, f-h). Arrows indicate vesicles fractured through completely, which reveals the inner surface of REVs.

a monochromatic neutron beam with a wavelength in the 1 nm to 3 nm range is scattered on the sample under investigation, and the scattered neutrons are detected on a 2D position sensitive detector. The primary information obtained by VSANS is the scattering curve, which is the radially averaged scattering intensity as the function of the momentum transfer (q), which is defined as $q = (4\pi/\lambda)sin\Theta$, where λ is the wavelength of the used neutron beam, and Θ is the half of the scattering angle. The measured scattering curves of the SSL 50, SSL 100 and REV samples are shown in Fig. 3a, which resembles the typical scattering curves of spherical particles. The so-called Guinier region, where a pronounced decrease in intensity as the function of q can be observed, carries information about the overall size of the particles. The shift of the Guinier region towards smaller q-values for the SSL 100 and REV samples indicate the increase in size of the scattering objects. Quantitative information from the scattering curves can be obtained by fitting of theoretical model functions to the measured curves. Since neutrons are scattered on the nuclei of the atoms of the scattering objects, the theoretical functions model the radial distribution of the neutron scattering cross section or neutron scattering length density (SLD) of the scattering objects. In our case, the scattering cross section difference between the deuterated solvent and the protonated phospholipid bilayer dominates the SLD profile of the vesicles, therefore SSLs were modelled with a spherical shell. In case of the REV sample, the SLD profile is different, because the SEC purification in the last step of the isolation replaces the outer buffer with PBS-D_2O, but the interior of REVs is filled with (protonated) macromolecules in normal aqueous buffer that represents almost no scattering contrast to the phospholipid bilayer. Therefore, REVs were modelled as homogeneous spheres, with a diameter representing the aqueous core together with the thickness of the lipid bilayer of REVs. In both cases, the size distributions of the liposomes and vesicles were taken into account with a log-normal distribution. Further details of the applied model functions and fitting procedures can be found in the Supplementary Information.

The fitted model functions are shown in Fig. 3a together with the measured scattering curves, and the corresponding size distribution are shown in Fig. 3b. The SSL 50, SSL 100 and REV samples were measured to have mean sizes (60.2 ± 0.3) nm, (84.1 ± 0.4) nm, and (175.4 ± 1.7) nm respectively. These diameter values are the smallest of the methods used in this study, an observation that is explained by the SLD profiles of SSLs and REVs. In case of SSLs, the hydrated PEG-chains represents the outer layer. Considering the concentration of the polymer, and the amount of D_2O in this layer, the average SLD of this layer is approximately $5.4 \cdot 10^{10}$ cm^{-2}, which does not represent a significant contrast to D_2O ($6.34 \cdot 10^{10}$ cm^{-2}) if one considers that the SLD of the protonated lipid bilayer is approximately $0.24 \cdot 10^{10}$ cm^{-2} (17). In other words, the size obtained from VSANS represents the outer diameter corresponding to the phospholipid headgroups. In case of REVs, the same holds for the protein corona based on the FF-TEM images, i.e. the average SLD contrast represented by the protein associates on the surface of REVs is negligible in a first approximation. With this assumption, the difference in the diameter from MRPS and VSANS carries information about the thickness of the PEG-layer in case of SSLs and the average thickness of the protein corona in case of REVs. For SSLs, this comparison results 5 nm to 6 nm for the thickness of the PEG-layer, which is just slightly larger than the values reported by SAXS (36,37). The same comparison for REVs implies the average thickness of the protein corona is (5.3 ± 0.3) nm, which is a reasonable approximation if one takes into account the density and size of the protein associates visible on the FF-TEM images.

Fig. 4 summarizes the size values obtained for the investigated samples by DLS, NTA, MRPS and VSANS. Clear trends can be observed for both the SSL and REV samples, which is attributed to the fact that different physical quantities are determined by the various techniques. The diameter determined by the boundary of the phospholipid bilayer is probed by VSANS, while MRPS determines the diameter equivalent to the excluded volume of the particles, which includes the PEG-layer in case of SSLs, and the protein corona, in case of REVs. The largest values were obtained by the optical methods, i.e. DLS, and NTA, which reports

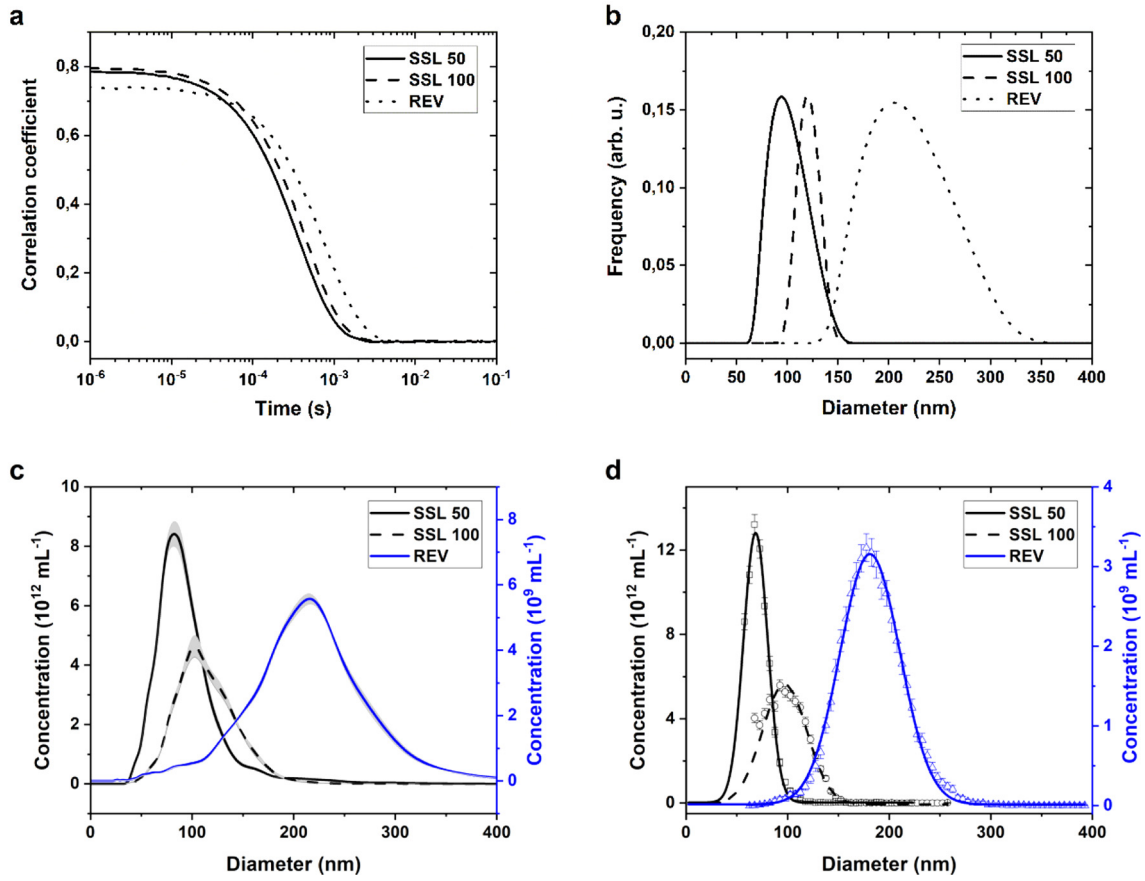

Fig. 2. DLS, NTA and MRPS analysis of SSL 50, SSL 100 and REV samples. (a) DLS correlation functions, and (b) the corresponding intensity weighted size distributions. (c) Number-based size distributions as determined by NTA. Shaded grey areas represent the standard deviation between measurements obtained from separate videos. (d) Number-based size distributions as determined by MRPS. Symbols and error bars represent concentration values with standard deviations, while solid lines correspond to fitted Gaussian functions.

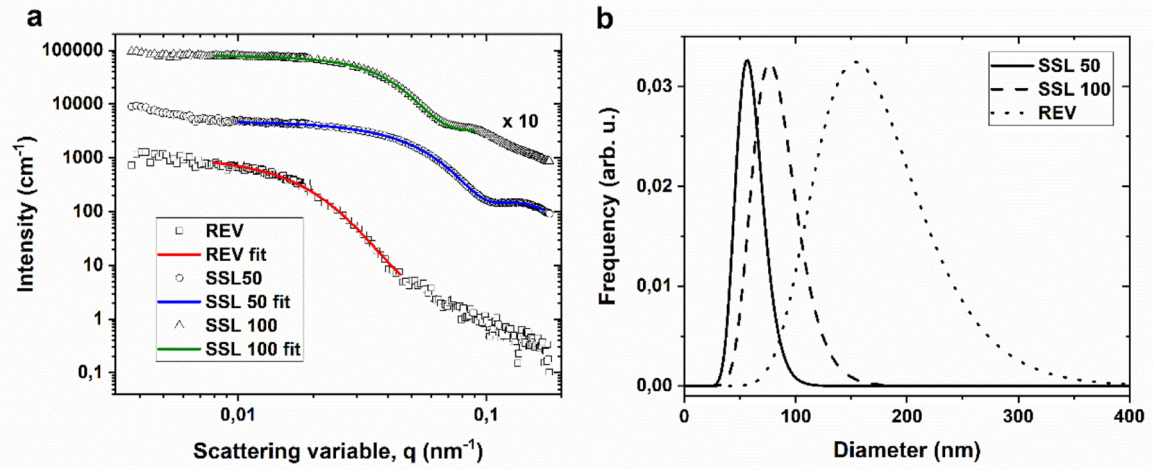

Fig. 3. VSANS analysis of SSL 50, SSL 100 and REV samples. (a) Measured scattering curves (symbols) and best fitting model functions (solid lines). Data points corresponding to the SSL 100 sample are shifted horizontally for better visibility. (b) Size distributions of the investigated samples corresponding to the best fitting models.

the equivalent diameter of a hard sphere with the same diffusion coefficient as the particles being measured. Both natural and synthetic lipid vesicle systems exhibit a pronounced hydration shell, which is also included in the size values reported by these techniques.

4. Conclusions

In this study four different sizing methods including DLS, NTA, MRPS and VSANS were used to characterize monodisperse synthetic and natural phospholipid vesicle systems. While each technique has its own limitations, the aim of this study was to gain further structural information about the samples by comparing the size values reported

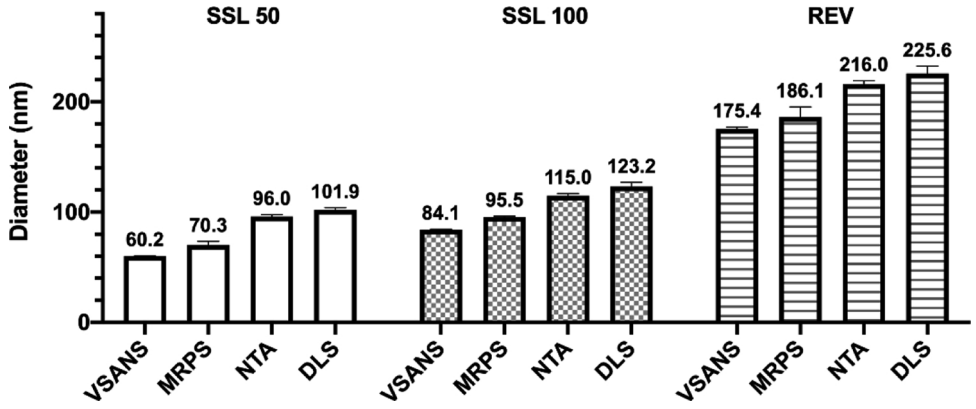

Fig. 4. Summary of the mean size values obtained for the investigated samples by DLS, NTA, MRPS and VSANS techniques.

by the different techniques. For this purpose, vesicle systems with monomodal size distributions were investigated in this study with mean sizes falling within the detection range of all the investigated methods. While drug delivery liposomes are commonly monodisperse in size, EV samples are most often very polydisperse so REVs were used as model EVs in this study.

By comparing optical methods that measure particle diffusion (DLS, NTA) with non-optical methods (MRPS, VSANS), significant differences can be observed in the reported mean diameters for the investigated samples. The differences indicate that the hydration shell of these soft colloidal particles can reach the thickness from 10 nm to 20 nm. The comparison of diameter values corresponding to the boundary of the phospholipid bilayer obtained from VSANS measurements with the values corresponding to the excluded volume of the particles by MRPS reveals the thickness of the PEG-layer in case of SSLs, and the thickness of the protein corona in case of REVs.

This study demonstrates the value of using orthogonal measurement techniques and that the comparison of carefully chosen sizing techniques can provide important structural information about the studied particles that cannot be obtained using one measurement alone.

CRediT authorship contribution statement

Zoltán Varga: Conceptualization, Investigation, Formal analysis, Writing - original draft, Writing - review & editing, Supervision, Funding acquisition. **Bence Fehér:** Formal analysis, Writing - original draft. **Diána Kitka:** Investigation. **András Wacha:** Formal analysis, Writing - original draft. **Attila Bóta:** Supervision, Writing - original draft. **Szilvia Berényi:** Investigation. **Vitaliy Pipich:** Investigation. **Jean-Luc Fraikin:** Writing - review & editing.

Declaration of Competing Interest

J-L. Fraikin is a co-founder of Spectradyne LLC, which developed the nCS1 instrument used in this study. All other authors declare no competing financial interests.

Acknowledgements

This work was supported by the National Research, Development and Innovation Office NKFIH, Hungary under grant numbers PD 121326 and NVKP_16-1-2016-0007. ZV was supported by the János Bolyai Research Fellowship. Part of this work is based upon experiments performed at the KWS-3 instrument operated by JCNS at the Heinz Maier-Leibnitz Zentrum (MLZ), Garching, Germany. ZV gratefully acknowledges the financial support provided by JCNS to perform the neutron scattering measurements at MLZ.

Appendix A. Supplementary data

Supplementary material related to this article can be found, in the online version, at doi:https://doi.org/10.1016/j.colsurfb.2020.111053.

References

[1] Y.C. Barenholz, Doxil®—the first FDA-approved nano-drug: lessons learned, Journal of controlled release 160 (2) (2012) 117–134.
[2] A.V. Vlassov, S. Magdaleno, R. Setterquist, R. Conrad, Exosomes: current knowledge of their composition, biological functions, and diagnostic and therapeutic potentials, Biochimica et Biophysica Acta. 1820 (2012) 940–948.
[3] E. van der Pol, A.N. Böing, P. Harrison, A. Sturk, R. Nieuwland, Classification, functions, and clinical relevance of extracellular vesicles, Pharmacological Reviews. 64 (2012) 676–705.
[4] S.E. Andaloussi, I. Mäger, X.O. Breakefield, M.J. Wood, Extracellular vesicles: biology and emerging therapeutic opportunities, Nature Reviews Drug Discovery. 12 (2013) 347–357.
[5] K.B. Johnsen, J.M. Gudbergsson, M.N. Skov, L. Pilgaard, T. Moos, M. Duroux, A comprehensive overview of exosomes as drug delivery vehicles — Endogenous nanocarriers for targeted cancer therapy, Biochimica et Biophysica Acta (BBA) - Reviews on Cancer. 1846 (August (1)) (2014) 75–87.
[6] K.B. Johnsen, J.M. Gudbergsson, M. Duroux, T. Moos, T.L. Andresen, J.B. Simonsen, On the use of liposome controls in studies investigating the clinical potential of extracellular vesicle-based drug delivery systems – A commentary, Journal of Controlled Release. 269 (January) (2018) 10–14.
[7] W. Jiang, R. Lionberger, X.Y. Lawrence, In vitro and in vivo characterizations of PEGylated liposomal doxorubicin, Bioanalysis. 3 (3) (2011) 333–344.
[8] S. Peretz Damari, D. Shamrakov, M. Varenik, E. Koren, E. Nativ-Roth, Y. Barenholz, et al., Practical aspects in size and morphology characterization of drug-loaded nano-liposomes, Int J Pharm. 547 (August (1–2)) (2018) 648–655.
[9] A. Nagayasu, K. Uchiyama, H. Kiwada, The size of liposomes: a factor which affects their targeting efficiency to tumors and therapeutic activity of liposomal antitumor drugs, Adv Drug Deliv Rev. 40 (November (1–2)) (1999) 75–87.
[10] C. Théry, K.W. Witwer, E. Aikawa, M.J. Alcaraz, J.D. Anderson, R. Andriantsitohaina, et al., Minimal information for studies of extracellular vesicles 2018 (MISEV2018): a position statement of the International Society for Extracellular Vesicles and update of the MISEV2014 guidelines, J Extracell Vesicles. 7 (1) (2018) 1535750.
[11] S.U. Egelhaaf, E. Wehrli, M. Adrian, P. Schurtenberger, Determination of the size distribution of lecithin liposomes: a comparative study using freeze fracture, cryoelectron microscopy and dynamic light scattering, Journal of Microscopy. 184 (3) (1996) 214–228.
[12] M.R. Brzustowicz, A.T. Brunger, X-ray scattering from unilamellar lipid vesicles, Journal of applied crystallography. 38 (2005) 126–131.
[13] S. Castorph, D. Riedel, L. Arleth, M. Sztucki, R. Jahn, M. Holt, et al., Structure parameters of synaptic vesicles quantified by small-angle X-ray scattering, Biophysical journal 98 (2010) 1200–1208.
[14] Z. Varga, Y. Yuana, A.E. Grootemaat, E. van der Pol, C. Gollwitzer, M. Krumrey, et al., Towards traceable size determination of extracellular vesicles, J Extracell Vesicles. 3 (2014) 23298.
[15] P. Balgavý, M. Dubnicková, N. Kucerka, M.A. Kiselev, S.P. Yaradaikin, D. Uhríková, Bilayer thickness and lipid interface area in unilamellar extruded 1,2-diacylphosphatidylcholine liposomes: a small-angle neutron scattering study, Biochim Biophys Acta. 1512 (May (1)) (2001) 40–52.
[16] M.A. Kiselev, S. Wartewig, M. Janich, P. Lesieur, M.A. Kiselev, M. Ollivon, et al., Does sucrose influence the properties of DMPC vesicles? Chem Phys Lipids 123 (März (1)) (2003) 31–44.
[17] L. Arleth, C. Vermehren, An analytical model for the small-angle scattering of polyethylene glycol-modified liposomes, Journal of Applied Crystallography. 43 (5 Part 1) (2010) 1084–1091.

[18] N. Arraud, R. Linares, S. Tan, C. Gounou, J.-M.-M. Pasquet, S. Mornet, et al., Extracellular vesicles from blood plasma: determination of their morphology, size, phenotype and concentration, Journal of Thrombosis and Haemostasis. 12 (5) (2014) 614–627.

[19] Y. Yuana, R.I. Koning, M.E. Kuil, P.C.N. Rensen, A.J. Koster, R.M. Bertina, et al., Cryo-electron microscopy of extracellular vesicles in fresh plasma, Journal of Extracellular Vesicles. 2 (January (1)) (2013) 21494.

[20] P. Cizmar, Y. Yuana, Detection and Characterization of Extracellular Vesicles by Transmission and Cryo-Transmission Electron Microscopy, in: W.P. Kuo, S. Jia (Eds.), Extracellular Vesicles [Internet], Springer New York, New York, NY, 2017, pp. 221–232 [cited 2019 Sep 18], Available from: http://link.springer.com/10.1007/978-1-4939-7253-1_18.

[21] Y. Yuana, T.H. Oosterkamp, S. Bahatyrova, B. Ashcroft, P. Garcia Rodriguez, R.M. Bertina, et al., Atomic force microscopy: a novel approach to the detection of nanosized blood microparticles, Journal of Thrombosis and Haemostasis. 8 (February (2)) (2010) 315–323.

[22] T. Bozó, T. Mészáros, J. Mihály, A. Bóta, M.S.Z. Kellermayer, J. Szebeni, et al., Aggregation of PEGylated liposomes driven by hydrophobic forces, Colloids and Surfaces B: Biointerfaces. 147 (November) (2016) 467–474.

[23] C. Chen, S. Zhu, T. Huang, S. Wang, X. Yan, Analytical techniques for single-liposome characterization, Anal Methods. 5 (9) (2013) 2150.

[24] F.A.W. Coumans, E. van der Pol, A.N. Böing, N. Hajji, G. Sturk, T.G. van Leeuwen, et al., Reproducible extracellular vesicle size and concentration determination with tunable resistive pulse sensing, J Extracell Vesicles. 3 (2014) 25922.

[25] R.A. Dragovic, C. Gardiner, A.S. Brooks, D.S. Tannetta, D.J. Ferguson, P. Hole, et al., Sizing and phenotyping of cellular vesicles using Nanoparticle Tracking Analysis, Nanomedicine: Nanotechnology, Biology and Medicine. 7 (2011) 780–788.

[26] C. Gardiner, Y.J. Ferreira, R.A. Dragovic, C.W. Redman, I.L. Sargent, Extracellular vesicle sizing and enumeration by nanoparticle tracking analysis, Journal of Extracellular Vesicles. 2 (2013) 19671, , https://doi.org/10.3402/jev.v2i0.19671.

[27] K. Vorauer-Uhl, A. Wagner, N. Borth, H. Katinger, Determination of liposome size distribution by flow cytometry, Cytometry. 39 (February (2)) (2000) 166–171.

[28] J.B. Simonsen, A liposome-based size calibration method for measuring microvesicles by flow cytometry, J Thromb Haemost. 14 (January (1)) (2016) 186–190.

[29] E. van der Pol, A.G. Hoekstra, A. Sturk, C. Otto, T.G. Van Leeuwen, R. Nieuwland, Optical and non-optical methods for detection and characterization of microparticles and exosomes, Journal of Thrombosis and Haemostasis. 8 (2010) 2596–2607.

[30] E.N. Hoen, E.J. van der Vlist, M. Aalberts, H.C. Mertens, B.J. Bosch, W. Bartelink, et al., Quantitative and qualitative flow cytometric analysis of nanosized cell-derived membrane vesicles, Nanomedicine: Nanotechnology, Biology and Medicine. 8 (5) (2012) 712–720.

[31] E. van der Pol, L. de Rond, F.A.W. Coumans, E.L. Gool, A.N. Böing, A. Sturk, et al., Absolute sizing and label-free identification of extracellular vesicles by flow cytometry, Nanomedicine. 14 (January (3)) (2018) 801–810.

[32] E. van der Pol, F a.W Coumans, A.E. Grootemaat, C. Gardiner, I.L. Sargent, P. Harrison, et al., Particle size distribution of exosomes and microvesicles determined by transmission electron microscopy, flow cytometry, nanoparticle tracking analysis, and resistive pulse sensing, J Thromb Haemost. 12 (July (7)) (2014) 1182–1192.

[33] J.-L.-L. Fraikin, T. Teesalu, C.M. McKenney, E. Ruoslahti, A.N. Cleland, A high-throughput label-free nanoparticle analyser, Nature Nanotechnology. 6 (May (5)) (2011) 308–313.

[34] A.D. Grabarek, D. Weinbuch, W. Jiskoot, A. Hawe, Critical Evaluation of Microfluidic Resistive Pulse Sensing for Quantification and Sizing of Nanometer- and Micrometer-Sized Particles in Biopharmaceutical Products, J Pharm Sci. 108 (January (1)) (2019) 563–573.

[35] G.V. Barnett, J.M. Perhacs, T.K. Das, S.R. Kar, Submicron Protein Particle Characterization using Resistive Pulse Sensing and Conventional Light Scattering Based Approaches, Pharm Res. 35 (February (3)) (2018) 58.

[36] Y. Schilt, T. Berman, X. Wei, Y. Barenholz, U. Raviv, Using solution x-ray scattering to determine the high-resolution structure and morphology of PEGylated liposomal doxorubicin nanodrugs, Biochimica et Biophysica Acta (BBA)-General Subjects. (2015).

[37] Z. Varga, A. Wacha, U. Vainio, J. Gummel, A. Bóta, Characterization of the PEG layer of sterically stabilized liposomes: a SAXS study, Chemistry and Physics of Lipids 165 (May (4)) (2012) 387–392.

[38] V. Pipich, Fu Z. KWS-3, Very small angle scattering diffractometer with focusing mirror. Journal of large-scale research facilities JLSRF [Internet], Aug 19 [cited 2019 Sep 23];1. Available from: (2015) http://jlsrf.org/index.php/lsf/article/view/28.

[39] G. Goerigk, Z. Varga, Comprehensive upgrade of the high-resolution small-angle neutron scattering instrument KWS-3 at FRM II, Journal of Applied Crystallography. 44 (April (2)) (2011) 337–342.